JOURNAL OF MATERIALS SCIENCE 29 (1994) 3913–3918

Structure, properties and response to heat treatment of melt-spun Al–Y and Al–La alloys

B. DILL*, Y. LI‡, M. AL-KHAFAJI, W. M. RAINFORTH, R. A. BUCKLEY, H. JONES
Department of Engineering Materials, University of Sheffield, Sheffield, S1 4DU, UK

Al–Y and Al–La binary alloys containing 0.7–18 wt% (0.2–6.3 at%) Y and 0.9–18 wt% (0.2–4.2 at%) La, were rapidly solidified by chill-block melt-spinning to produce ribbons between 35 and 70 μm thick. Microstructures were of the classical zone A/zone B type with a notable increase in αAl lattice parameter for the Al–6.3 at% Y composition, which exhibited a Knoop hardness of 430 ± 30 kg mm^{-2} as-spun. Isochronal ageing for 2 h at 200–500 °C gave significant hardening at 200 and/or 300 °C for all of the more concentrated alloys, the largest responses being produced by Al–6.3 at% Y and Al–4.2 at% La at 200 °C. X-ray diffraction as-spun indicated the presence of only αAl and equilibrium $Al_{11}La_3$ in the Al–La alloy ribbons and αAl and a non-equilibrium $Al_4Y/Al_{11}Y_3$ in the Al–Y ribbons. This non-equilibrium Al–Y phase was identified by X-ray diffraction as isomorphous with orthorhombic or tetragonal $Al_{11}La_3$ with lattice parameters determined as $a_0 = 0.42 \pm 0.02$ nm ($b_0 = 1.26 \pm 0.06$ nm) and $c_0 = 0.97 \pm 0.05$ nm. TEM showed that it was present as an intercellular network with Energy dispersive spectroscopic analysis indicating an average composition Al–46 wt% Y consistent with the $Al_4Y/Al_{11}Y_3$ stoichiometry and diffraction patterns consistent with an orthorhombic or tetragonal cell with these lattice parameters. While no significant change in phase constitution of the Al–La ribbons was detected by X-ray diffraction as a result of heat treatment, the $Al_{11}Y_3$ in Al–Y ribbons was seen to be replaced by βAl_3Y on heat treatment at 400 and 500 °C.

1. Introduction

Although the effects of transition metal additions on the structure and thermal stability of rapidly solidified aluminium-base alloys is now very well documented (see, for example, [1–3]), the corresponding effects of yttrium and lanthanide (i.e. rare earth, RE) additions did not begin to be reported systematically until the mid-eighties (see, for example, [4–7]). In such systematic studies for 20 μm thick chill-block melt-spun Al–RE alloy ribbons, Inoue *et al.* [8, 9] found that crystalline solid solutions based on f c c αAl formed up to 7–9 at % RE, then an amorphous phase up to 10–17 at % RE, above which unidentified or equilibrium crystalline intermetallic phases began to feature. Only limited attention has been given, however, to the crystalline αAl-based microstructures formed by rapid solidification at RE contents below the 8 ± 1 at % RE level required to form the amorphous phase, in spite of the potential of such αAl-based microstructures for the development of new engineering alloys for high-temperature applications. Characterization of the αAl-based crystalline microstructures based on Al–Y and Al–La have been particularly sparse [6, 7, 10–14] so these were selected for the present study.

2. Experimental procedure

Alloys with nominally 1, 3, 10 and 20 wt % Y or La were made by vacuum induction melting of 99.999 wt % Al and 99.99 wt % Y or La and casting under argon into rectangular ingots of dimensions 16 mm × 50 mm × 150 mm in a steel mould. Resulting alloy compositions are indicated in Table I. Samples (10 g) of each alloy were chill-block melt-spun at 180 K superheat on a copper wheel at 29 m s^{-1} (also 46 m s^{-1} for alloy Y10) from quartz crucibles to give ribbon between 35 and 70 μm thick. Isochronal heat treatments of resulting ribbon were carried out in quartz ampoules that had been evacuated prior to back-filling with argon. These furnace treatments were for 2 h at 200, 300, 400 and 500 °C and were terminated by water quenching. X-ray diffractometry (XRD) employed Co$K\alpha$ and Cu$K\alpha$ radiations. Samples were also characterized through thickness by optical, scanning and transmission electron microscopy. Thinning for TEM and energy dispersive spectroscopy (EDS) on a Philips 400T electron microscope was carried out from free, wheel or both sides of ribbons using GATAN ion-milling equipment. Microhardness measurements were made on polished and etched

* *Permanent address*: University of Erlangen, Erlangen, Germany.
‡ *Present address*: Department of Physics, National University of Singapore.

TABLE I Ingot composition, constitution as-spun, αAl lattice parameter and microhardness of Al–Y and Al–La alloys studied

Alloy symbol	Ingot composition		Constitution as-spun		αAl lattice parameter (pure Al = 0.404 94 nm)	Microhardness (Knoop) (kg mm^{-2}) (pure Al = 40 kg mm^{-2})
	wt % Y or La	at % Y or La	Optical	XRD[a]		
Y1	0.7Y	0.2Y	Zone B	P_1	0.404 99	47 ± 7
Y3	2.4Y	0.7Y	Zone B	$P_1 + P_2$	0.404 98	76 ± 20
Y10	9.4Y	3.1Y	Zones B + A	$P_1 + P_2$	0.405 11, 0.405 26[b]	123 ± 27, 210 ± 20[c]
Y20	18.2Y	6.3Y	Zone A	$P_1 + P_2$	0.408 18	430 ± 30[c]
La1	0.9La	0.2La	Zone B	P_1	0.404 96	53 ± 6
La3	2.6La	0.5La	Zone B	$P_1 + P_2$	0.404 99	67 ± 5
La10	9.9La	2.1La	Zones B + A	$P_1 + P_2$	0.405 04	108 ± 12, 157 ± 16[c]
La20	18.4La	4.2La	Zones B + A	$P_1 + P_2$	0.405 13	250 ± 30, 310 ± 20[c]

[a] $P_1 = \alpha Al$, $P_2 = Al_4X/Al_{11}X_3$.
[b] Spun at 46 m s^{-1}.
[c] Zone A

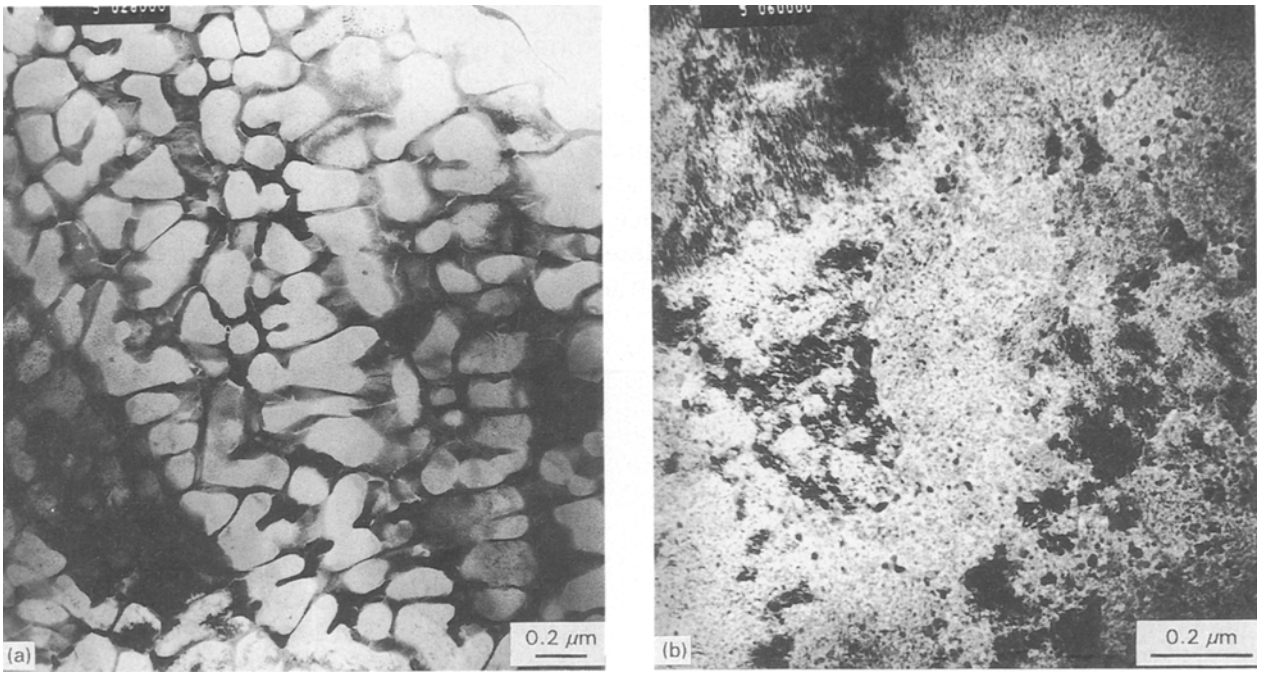

Figure 1 Bright-field transmission electron micrographs of (a) zone B and Y10 as-spun, compared with (b) zone A in La20 as-spun.

resin-mounted ribbon cross-sections using a Knoop (HK 0.01/10s) indentor. Each resulting measurement is the average from a minimum of ten indentations on the same sample.

3. Results

3.1. As-spun condition

Optical microscopy on polished and etched ribbon cross-sections, as-spun, showed microsegregated zone B [15] type structures at the lower yttrium or lanthanum contents with an increasing presence of featureless zone A [15] type structure at the chill side with increasing alloying content, the proportion of zone A reaching 100% only for alloy Y20, which also showed the highest microhardness (Knoop 430 ± 30 kg mm^{-2}) (Table I). Correspondingly, XRD

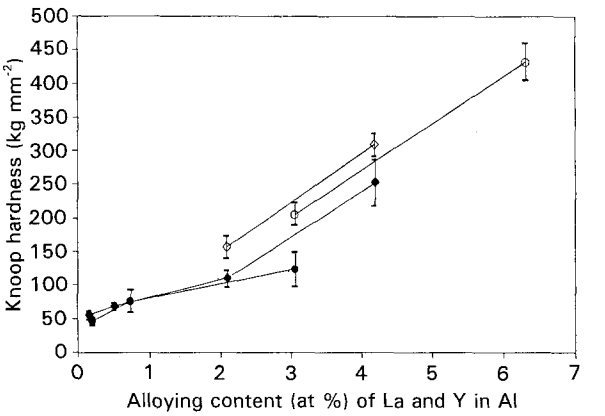

Figure 2 Knoop microhardness (HK 0.01) of Al–Y and Al–La as-spun versus alloying content. (○) Al–Y zone A, (●) Al–Y zone B, (◇) Al–La zone A, (◆) Al–La zone B.

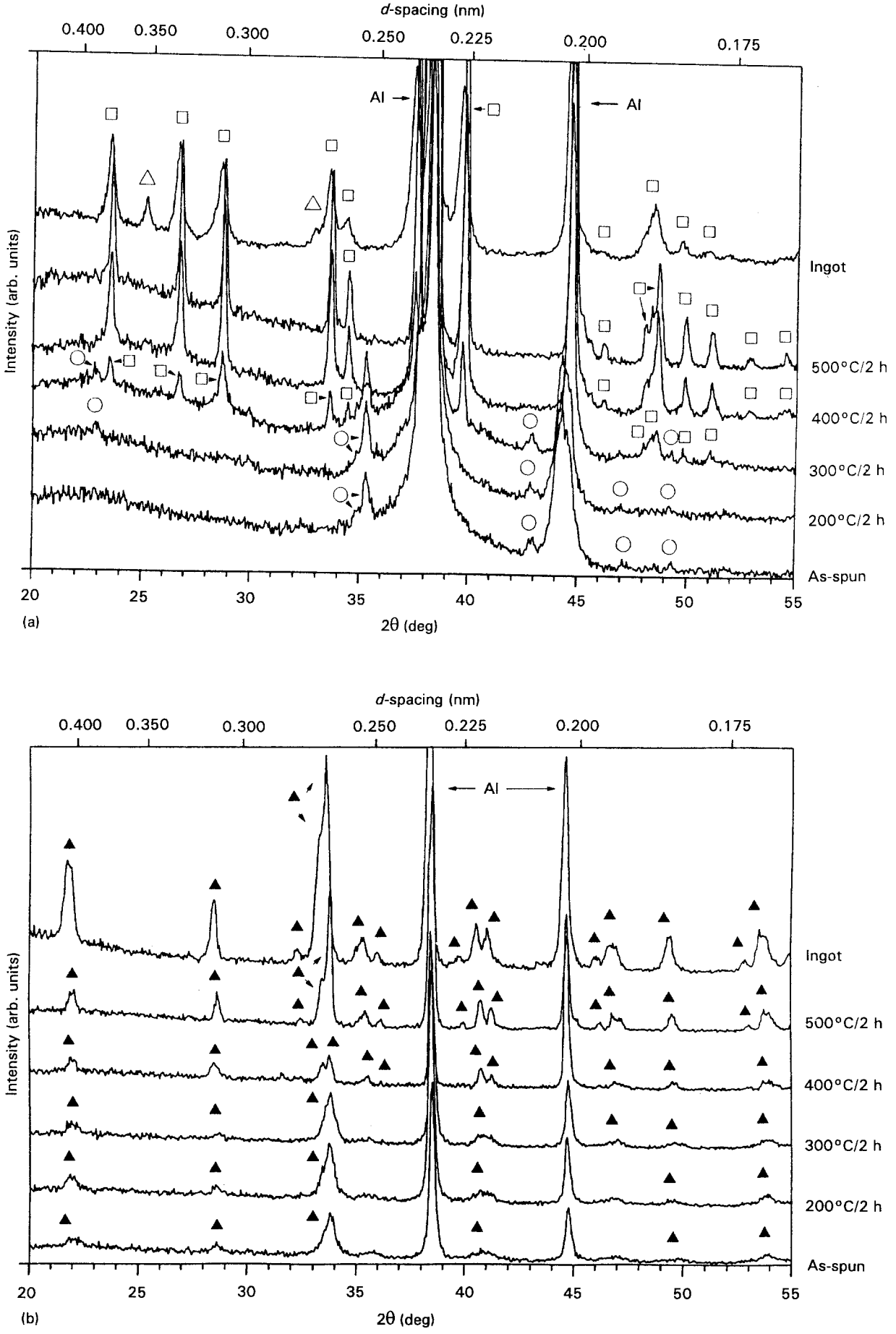

Figure 3 XRD traces showing the effects of heat treatment on the constitution of melt-spun alloys, (a) Y20 and (b) La20. (△) α-Al_3Y, (□) β-Al_3Y, (○) Al_4Y, (▲) $Al_{11}La_3$.

TABLE II Effect of isochronal (2 h) treatment at 200–500 °C on αAl lattice parameter for Y10, Y20 and La20 ribbons

Treatment	αAl lattice parameter (nm)		
	Alloy Y10	Alloy Y20	Alloy La20
As-spun	0.405 11 ± 0.000 02	0.408 18 ± 0.000 32	0.405 13 ± 0.000 03
200 °C/2 h	0.405 07 ± 0.000 05	0.407 85 ± 0.000 22	0.405 11 ± 0.000 02
300 °C/2 h	0.405 07 ± 0.000 02	0.405 17 ± 0.000 03	0.405 11 ± 0.000 03
400 °C/2 h	0.405 04 ± 0.000 03	0.405 16 ± 0.000 02	0.405 08 ± 0.000 03
500 °C/2 h	0.405 02 ± 0.000 01	0.405 03 ± 0.000 07	0.405 09 ± 0.000 03

showed αAl with increasing incidences of $Al_4Y/Al_{11}Y_3$ or $Al_{11}La_3$ [16] with increase in yttrium or lanthanum content as-spun. The lattice parameter of αAl showed small increases with increased alloy content up to the Y10 and La20 levels with a step increase between Y10 and Y20 corresponding to the complete displacement of zone B by zone A for Y20. TEM showed equiaxed αAl grain sections containing fine (30 nm) spheroidal precipitates for Y1, compared with increasingly refined cellular αAl with continuous intercellular second phase for Y3, Y10 and Y20.

Fig. 1a and b compare the cellular structure of zone B in Y10 as-spun with that of zone A in La20 which show αAl with an array of fine precipitates of size ~ 10 nm. Cellular zone B in La20 as-spun contained, in addition, primary intermetallic particles up to 0.5 μm in size. Careful selected-area diffraction (SADP) and EDS analysis of the intercellular network phase in Y10 identified it as orthorhombic $Al_4Y/Al_{11}Y_3$ containing 54 wt % Y, with $a_0 = 0.42 \pm 0.02$ nm, ($b_0 = 0.97 \pm 0.05$ nm) and $c_0 = 1.26 \pm 0.06$ nm. SADP, similarly, identified the primary intermetallic in zone B and the fine precipitates in zone A of La20 as $Al_{11}La_3$ [13]. Microhardness increased monotonically with increasing alloy content for both zones A and B, the increment in hardness associated with zone A being ~ 100 kg mm^{-2} for Al–Y and ~ 50 kg mm^{-2} for Al–La (Fig. 2).

3.2. Effects of heat treatment

While heat treatment for 2 h at 200 or 300 °C had no detectable effect on etching response, treatment at 400 or 500 °C resulted in a marked response, for example, from what was previously zone A in Y10 or Y20. XRD showed a systematic development of any $Al_4X/Al_{11}X_3$ (X = Y or La) peaks present as-spun with increase in treatment temperature, with displacement of $Al_4Y/Al_{11}Y_3$ by β-Al_3Y for Al–Y samples treated at 500 °C. Examples for Y20 and La20 are shown in Fig. 3a and b. Correspondingly, the lattice parameter of the αAl matrix decreased detectably with increase in treatment temperature as indicated in Table II (with a large decrease for Y20 between 200 and 500 °C) while microhardness decreased systematically as a result of treatments at 300, 400 and 500 °C, offsetting the effect of any detectable hardening as a result of treatment at 200 or 300 °C (Fig. 4a, b). TEM of Y10, Y20 and La20 samples treated at 300 and 400 °C showed evidence of staged dissolution of the $Al_4X/Al_{11}X_3$ zone B network to be replaced by necklace-like βAl_3Y in Y20 ribbon treated for 2 h at 400 °C (Fig. 5a and b).

4. Discussion

$Al_{11}La_3$ is the most aluminium-rich equilibrium intermetallic phase of the Al–La system [17] so its presence as the only detected second phase in as-spun Al (2–18 wt % La) is not unexpected. The corresponding phase $Al_4Y/Al_{11}Y_3$ found in as-spun Al (3–18 wt % Y), however, is not an equilibrium phase of the Al–Y system [18], and so should be replaced by equilibrium Al_3Y on heat treatment, in accord with our results. The occurrence of metastable $Al_4Y/Al_{11}Y_3$ has been reported recently by Li *et al.* [12, 13] in melt-spun Al–10 at % Y for wheel speeds below 40 m s^{-1} and as a product of crystallization of the metallic glass formed above 40 m s^{-1}. Kim *et al.* [14], however, reported the formation of αAl and Al_3Y in Al (2–6 at % Al) ribbons spun at 42 m s^{-1}. The effect of increasing yttrium and lanthanum content in increasing the lattice parameter, a_0, of the αAl solid solution is expected

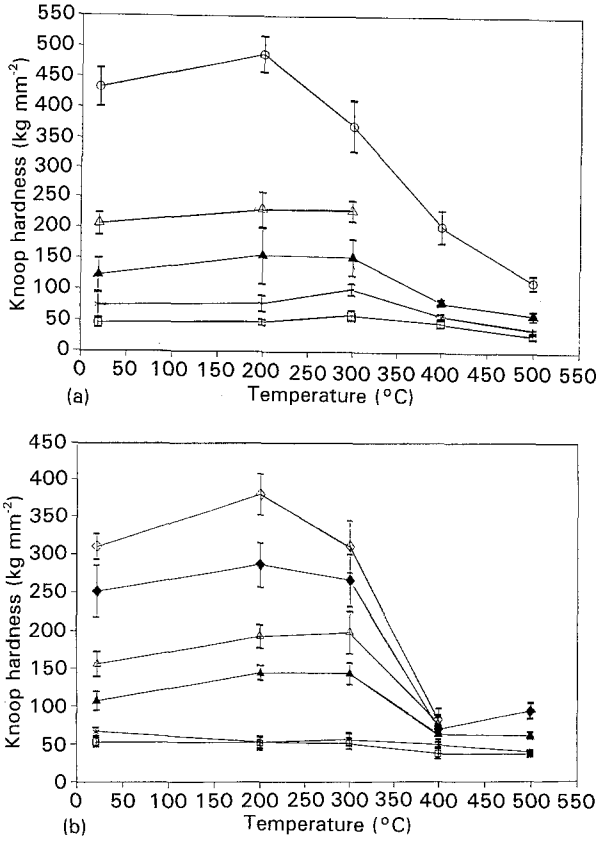

Figure 4 Knoop microhardness (HK 0.01) versus temperature of 2 h heat treatment for melt-spun (a) Al–Y and (b) Al–La alloys. (a) (□) Y1 zone B, (*) Y3 zone B, (▲) Y10 zone B, (△) Y10 zone A, (○) Y20 zone A. (b) (□) La1 zone B, (*) La3 zone B, (▲) La10 zone B, (△) La10 zone A, (◆) La20 zone B, (◇) La20 zone A.

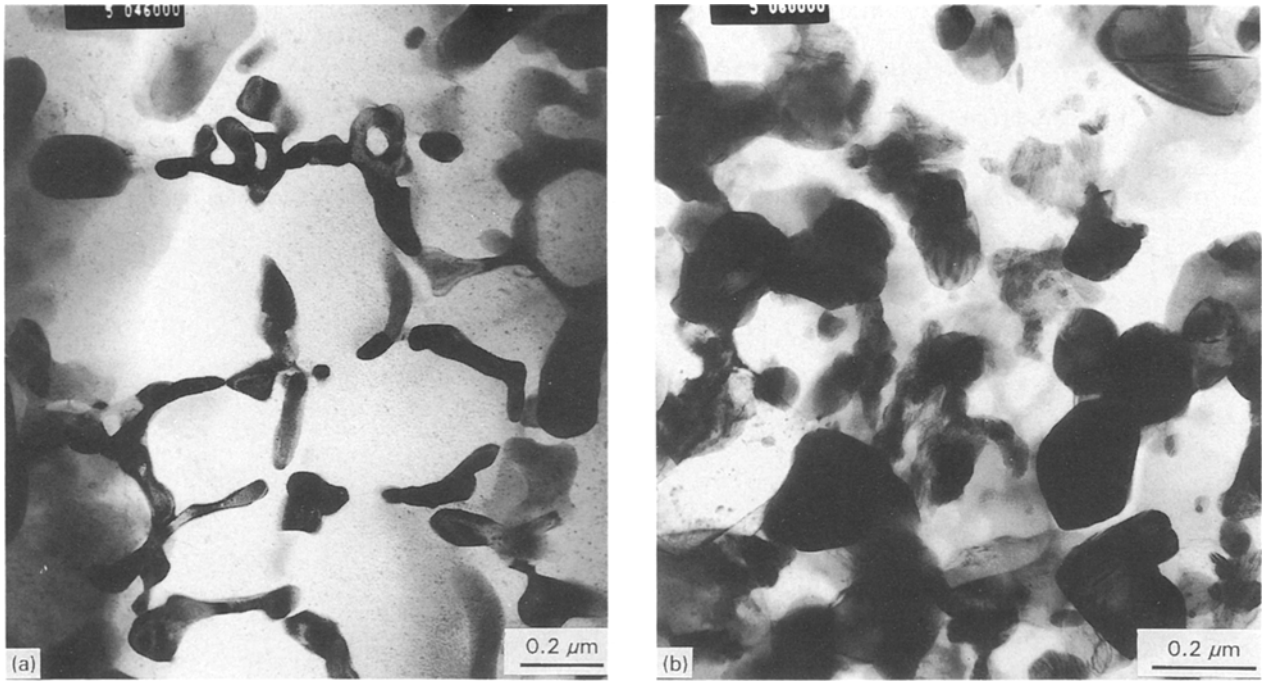

Figure 5 Bright-field transmission electron micrographs showing the effect of heat treatment for 2 h at 400 °C: (a) Y10, partial dissolution of $Al_4Y/Al_{11}Y_3$ network in zone B; (b) Y20, necklace-like βAl_3Y, replacing $Al_4Y/Al_{11}Y_3$.

on the basis of the larger atomic radii of yttrium and lanthanum than aluminium. Our results for the magnitude of the effect for yttrium are in good agreement with those of Kim *et al.* [14]. The magnitude of the apparent effect $(1/a_0)(da_0/dc)$ where c is alloy concentration (atom fraction) is $\sim +0.127$ for yttrium and $+0.012$ for lanthanum is similar to that [19] for scandium in αAl, which, as for yttrium and lanthanum, has a larger atomic size than aluminium. The increased incidence of the "zone A" microstructure with increasing yttrium and lanthanum content is in the opposite sense to that found, for example, for rapidly solidified Al–Fe alloys, achieving 100% incidence at 6.3 at % Y in the case of the Al–Y ribbons. The hardening rate, dH/dc, of $\sim 70\,kg\,mm^{-2}$ per at % associated with zone A in both Al–Y and Al–La, however, is similar to that for zone A in Al–Fe and accords with the results of Kim *et al.* [14] for comparable Al–Y. The significant age-hardening effects shown in Fig. 4a and b are, of course, additional and presumably arise from precipitation from the extended solid solutions of yttrium and lanthanum in αAl leading to the reduction of αAl lattice parameter recorded in Table II. Fig. 4a and b indicate a good measure of thermal stability of the hardening mechanism for the 2–4 at % Y and La levels that might form the basis of an engineering alloy formulation. Excellent treatments of the mechanism of hardening in such zone A rapidly solidified aluminium alloy microstructures have been given by Fontaine [20] and Dermarkar [21].

5. Conclusions

1. Rapid solidification of Al (0.2–6.3 at % Y) and Al (0.2–4.2 at % La) alloys by chill-block melt-spinning produces zone A/B type microstructures analogous in many respects to those produced by rapid solidification of comparable Al–Fe alloys.

2. The $Al_4X/Al_{11}X_3$ (X = Y or La) which was present in the αAl matrix as-spun is metastable in the case of Al–Y ribbons and reverts to the equilibrium βAl_3Y phase on treatment at elevated temperature.

3. The rate of increase of αAl lattice parameter as-spun with increasing yttrium or lanthanum content is in accord with expectation for such solutes with atomic radius larger than that of the aluminium atoms forming the solvent lattice.

Acknowledgements

Bernhard Dill is grateful to the University of Erlangen for the financial support that enabled him to carry out this work at the University of Sheffield which is associated with a programme supported by the UK Science and Engineering Research Council.

References

1. T. R. ANANTHARAMAN, P. RAMACHANDRARAO, C. SURYANARAYANA, S. LELE and K. CHATTOPADHYAY, *Trans. Ind. Inst. Metals* **30** (1977) 434.
2. J. KANEKO, T. MURAKAMI and N. FURUSHIRO, *J. Jpn Inst. Metals* **39** (1989) 147.
3. H. JONES, *Philos Mag. B* **61** (1990) 487.
4. S. J. SAVAGE and F. H. FROES, in "Rapidly Solidified Metastable Materials", edited by B. H. Kear and B. C. Griessen (Elsevier Science, NY, 1984) pp. 329–33.
5. M. X. QUAN, P. HALDAR, J. WERTH and B. C. GIESSEN, in "Rapidly Solidified Alloys and their Mechanical and Magnetic Properties", edited by B. C. Griessen, D. Polk and A. I. Taub (MRS, Pittsburgh, PA, 1986) pp. 299–304.
6. A. RUDER and D. ELIEZER, *Israel J. Technol.* **24** (1988) 149.
7. A. INOUE, K. OHTERA and T. MASUMOTO, *Jpn J. Appl. Phys.* **27** (1988) L736.
8. *Idem, Sci. Rep RITU-A* **35** (1990) 115.

9. A. INOUE, M. WATANABE, H. KIMURA and T. MASUMOTO, *ibid.* **36** (1991) 59.
10. A. RUDER and D. ELIEZER, *J. Mater. Sci. Lett.* **8** (1989) 725.
11. *Idem, J. Mater. Sci.* **24** (1989) 1474.
12. Q. LI, E. JOHNSON, A. JOHANSEN and L. SARHOLT-KRISTENSEN, *J. Mater. Res.* **7** (1992) 2756.
13. Q. LI, E. JOHNSON, M. B. MADSEN, A. JOHANSEN and L. SARHOLT-KRISTENSEN, *Philos. Mag. B* **66** (1992) 427.
14. Y.-H. KIM, A. INOUE and T. MASUMOTO, *Mater. Trans. JIM* **32** (1991) 331.
15. H. JONES, *Mater. Sci. Eng.* **5** (1969) 1.
16. A. H. GOMES DE MESQUITA and K. H. J. BUSCHOW, *Acta Crystallogr.* **22** (1967) 497.
17. K. A. GSHNEIDNER Jr and F. W. CALDERWOOD, *Bull. Alloy Phase Diagrams* **9** (1988) 686.
18. *Idem, ibid.* **10** (1989) 44.
19. H. JONES, *Scripta Metall.* **17** (1983) 97.
20. A. FONTAINE, in "Rapidly Quenched Metals", edited by N. J. Grant and B. C. Giessen (MIT Press, Cambridge, MA, 1976) pp. 163–7.
21. S. DERMARKAR, in "Rapidly Solidified Powder Metallurgy Aluminium Alloys", edited by M. E. Fine and E. A. Starke Jr, ASTM STP 890 (American Society for Testing and Materials, Philadelphia, PA, 1986) pp. 154–65.

Received 2 February
and accepted 16 February 1994